

<https://doi.org/10.1038/s41612-024-00613-5>

# Unveiling the dynamics of sequential extreme precipitation-heatwave compounds in China

Check for updates

Lijuan Miao<sup>1</sup>, Lei Ju<sup>1</sup>, Shao Sun<sup>2</sup>, Evgenios Agathokleous<sup>3</sup>, Qianfeng Wang<sup>4</sup>, Zhiwei Zhu<sup>5</sup>, Ran Liu<sup>1</sup>, Yangfeng Zou<sup>1</sup>, Yutian Lu<sup>1</sup> & Qiang Liu<sup>6</sup>✉

Amidst the escalating impacts of global warming, the occurrence and severity of compound extreme weather events have risen significantly, presenting substantial threats to both lives and property. Existing response strategies predominantly focus on individual events, often overlooking the cumulative effects rising from their inherent complexity. To address this critical gap, we conducted a thorough examination of sequential extreme precipitation–heatwave compound events (SEPHCE) in China from 1975 to 2020, utilizing data from 1929 meteorological stations. Our investigation revealed a consistent rise in the frequency and duration of SEPHCE, with a particularly notable surge since 1993. Furthermore, shorter interval events disproportionately affected the regions of southwestern and southeast coastal China. Furthermore, SEPHCE onset times exhibited advancement, and the endings were delayed, thereby intensifying the overall trend. These findings underscore the pressing need to prioritize effective planning and adaptation strategies to mitigate the impact of these compound event, while also addressing the potential exacerbation of inequality resulting from climate change.

The discernible increase in the frequency and severity of climate extremes, attributed to global warming<sup>1–3</sup>, has resulted in catastrophic impacts for both human life and the ecological environment across various regions<sup>4,5</sup>. Among these adversities, heatwaves and extreme precipitation stand out as two of the most widespread and recurrent extreme events, inflicting significant harm on human societies and ecosystems<sup>6,7</sup>. Notably, floods and geological disasters in China affected 51.9 million people, resulting in direct economic losses totaling up to 239.3 billion in 2023<sup>8</sup>. In summer 2022, heatwave events affected 38.3 million people<sup>9</sup>.

The concept of compound events, initially introduced in the IPCC Fifth Assessment Report, has been further defined and expanded in IPCC AR6<sup>4,10</sup>. This includes compound events involving antecedent events, multivariate events, time compound events, and spatial compound events<sup>4</sup>. It is recognized that the impacts of spatial and/or temporal compound events often far exceed those of single events and their cumulative effects<sup>11,12</sup>. Consequently, there is a high focus on understanding the changes and characteristics of sequential extreme precipitation–heatwave compound events (SEPHCE), which are crucial for preventing and mitigating natural

disasters, ensuring economic development, and securing human well-being<sup>13</sup>. This focus is not only pertinent in the present but also constitutes a crucial element in addressing the challenges posed by climate change in the future<sup>14</sup>.

Since the 1950s, high-temperature events and extreme precipitation have risen worldwide<sup>6,7</sup>. Over recent decades, climate change-induced hazards, such as floods and heatwaves, have increased fivefold, resulting in over two million deaths and economic cost losses exceeding \$3.64 trillion<sup>7,15–18</sup>. As interest in this field continues to grow, an expanding community of scholars are delving into the dynamics and attributions of compound events. One example is the flood-heatwave event that struck western Japan in summer 2018, resulting in a tragic loss of thousands of lives within just 1 week<sup>19,20</sup>. Similarly, in the central United States, the occurrence of extreme precipitation following summer heatwaves frequently triggers floods, posing significant challenges to food security and ultimately threatening human livelihoods<sup>14</sup>.

Concurrently, research has explored the probability and evolving characteristics of compound heatwave and flood events<sup>21</sup>. Heavy rainfall is

<sup>1</sup>School of Geographical Sciences, Nanjing University of Information Science and Technology, Nanjing, China. <sup>2</sup>State Key Laboratory of Severe Weather, Chinese Academy of Meteorological Sciences, Beijing, China. <sup>3</sup>School of Applied Meteorology, Nanjing University of Information Science and Technology, Nanjing, China. <sup>4</sup>College of Environment and Safety Engineering, Fuzhou University, Fuzhou, China. <sup>5</sup>School of Atmospheric Sciences, Nanjing University of Information Science and Technology, Nanjing, China. <sup>6</sup>School of Remote Sensing and Geomatics Engineering, Nanjing University of Information Science and Technology, Nanjing, China. ✉e-mail: [qiang.liu@nuist.edu.cn](mailto:qiang.liu@nuist.edu.cn)

more likely to occur shortly after shorter and hotter heatwaves<sup>21</sup>. In contrast to the simultaneous occurrence of heatwaves and droughts, heatwaves and extreme precipitation events are typically isolated<sup>22</sup>. However, with the intensification of climate change, the probability of their convergence may intensify<sup>23,24</sup>.

While previous research has primarily focused on countries such as the United States and Japan, where the incidence of compound events is notably high<sup>25,26</sup>. The rapid urbanization witnessed in China since the 1970s has exacerbated the frequency, duration, and intensity of extreme weather and climate events<sup>27,28</sup>. To better assess and mitigate the impacts and risks that societal expansion into the environment may bring, it is imperative to thoroughly investigate and evaluate the occurrence and evolution of SEPHCE in China<sup>29</sup>. Such an endeavor will contribute to the formulation of effective response strategies, ensuring the sustainable development of society and the environment<sup>30</sup>.

In the examination of extreme weather characteristics, multiple indicators have been proposed<sup>31–33</sup>, including frequency, duration, and intensity<sup>16,21</sup>. Some researchers, utilizing the definition of daily maximum and minimum temperatures, have investigated the variations in the intensity, frequency, and duration of heatwaves in North America and Europe<sup>34</sup>. For European heatwaves, specific criteria such as temperatures exceeding the 90th percentile of maximum temperatures during the heatwave for at least 6 days were set, and a series of heatwave indices were systematically defined<sup>35,36</sup>. These indices describe the characteristics of heatwaves, including the total number of heatwave days in summer, the frequency of heatwave occurrences, the duration of heatwaves, and the average maximum amplitude of heatwaves.

However, with global warming, increasing reports of extreme weather arriving earlier and setting historical records have captured people's attention<sup>37</sup>. This has prompted considerations of the societal collapse risks associated with the early onset of future extreme weather. Therefore, the study of the start and end times of historical SEPHCE periods has become particularly important. This represents an innovative attempt to calculate the characteristics of SEPHCE, aiming to provide timely predictions and warnings to reduce casualties and property damage. This forward-looking research contributes to a better understanding and preparation for potential future climate extremes.

Here we explore the historical evolution patterns and characteristics of SEPHCE in China. Utilizing data from 1929 meteorological stations, we identified SEPHCE in China from 1975 to 2020. A comprehensive analysis of SEPHCE includes aspects such as frequency, duration, start and end times, as well as the probability distribution of joint intensity. It is noteworthy that this study represents the first systematic and comprehensive assessment of SEPHCE against the backdrop of climate change. Through this research, we aim to provide support for the development of targeted and effective risk and climate adaptation strategies.

## Results

### Temporal and spatial trends of SEPHCE frequency in China

The frequency of SEPHCE exhibited a significant and consistent increase from 1975 to 2020, with varying rates observed at intervals of 1, 3, 5, and 7 days measured at 17, 67, 122, and 176 occurrences per decade, respectively

(Supplementary Fig. 1). Between 1975 to 1992, SEPHCE frequencies remained relatively stable, with occurrences at intervals of 1, 3, 5, and 7 days fluctuating around 10, 53, 108, and 167, respectively. From 1993 to 2020, SEPHCE frequencies saw significantly upturn, with occurrences at intervals of 1, 3, 5, and 7 days reaching peak values of 149, 494, 826, and 1175, respectively, within a year (Fig. 1a), showing growth rates of 30, 107, 179, and 258 occurrences per decade, respectively. In Fig. 1b, the ratio of mean SEPHCE frequencies in the most 10 years compared to the previous 10 years initially increased gradually from 1.2 times to 1.8 times (1975–2014). In the last period (2015–2020), occurrences at intervals of 3, 5, and 7 days showed a slight decrease, while SEPHCE occurring with an 1-day interval continued to grow, reaching more than twice mean frequencies of the previous decade (1995–2014; Fig. 1b).

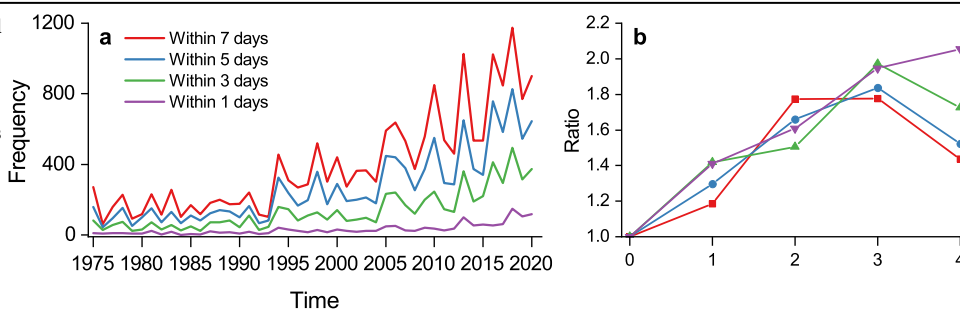
The annual SEPHCE frequency data were spatially interpolated into a grid with 0.1° resolution, covering mainland China. The spatial patterns of SEPHCE frequency in China between 1975 and 2020 revealed significant regional variations (Fig. 2a–d). SEPHCE at intervals of 3, 5, and 7 days displayed relatively consistent spatial distribution features, with higher frequencies predominantly concentrated in the southwestern and southern coastal regions of China, while lower frequencies were located in the northern regions (Fig. 2a–c). Specifically, SEPHCE at the 7-day interval were more frequent in the southwestern region, with up to 30 occurrences (Fig. 2a). The southeastern coastal region experienced between 12 and 18 occurrences, while other regions had fewer SEPHCE occurrences, ranging from 6 to 12 (Fig. 2a). In contrast, SEPHCE at 5-day and 3-day intervals occurred approximately 15 and 9 times, respectively, in southwestern China (Fig. 2b, c). For SEPHCE at an 1-day interval, the recorded occurrences ranged between 2 and 6 times in the southwestern region (Fig. 2d).

The spatial trends of SEPHCE frequency in China from 1975 to 2020 revealed distinctive spatial variations (Fig. 3). Overall, SEPHCE frequency exhibited a more rapid increase in the southwestern and southern coastal regions, while other regions exhibited a relatively slower rate of increase (Fig. 3). The spatial trends in SEPHCE frequency exhibited similar distribution patterns at both 7-day and 5-day intervals, mainly concentrated in the southwestern and southeastern coastal regions (Fig. 3a, b). In southwestern China, the growth rates of SEPHCE frequency at the 7-day and 5-day intervals ranged from 0.18 to 0.30 occurrences per decade and from 0.06 to 0.18 occurrences per decade, respectively (Fig. 3a, b). However, the growth trend in SEPHCE frequency at the 3-day and 1-day intervals was not statistically significant, with rates ranging from 0.06 to 0.12 occurrences per decade for the 3-day interval and below 0.06 occurrences per decade for the 1-day interval (Fig. 3c, d).

### Temporal and spatial trends of SEPHCE duration in China

A continuous and rapid increase in SEPHCE duration across China from 1975 to 2020 was evident (Fig. 4). Specifically, the increasing rates at the intervals of 1, 3, 5, and 7 days were 113, 424, 765, and 1117 days per decade, respectively (Supplementary Fig. 2). SEPHCE duration remained relatively stable between 1975 and 1992 at intervals of 1, 3, 5, and 7 days, fluctuating with corresponding durations of 50, 258, 533, and 835 days, respectively (Fig. 4a). However, a significant acceleration in the growth rate of SEPHCE duration became evident from 1993 to 2020 (Fig. 4a). The most substantial

**Fig. 1 | Annual variations of SEPHCE (sequential extreme precipitation–heatwave compound events) frequencies in China from 1975 to 2020.** a The annual SEPHCE frequencies; b the ratios of the mean SEPHCE frequencies in the latter 10 years to the former 10 years. Due to data limitations, the last mean ratio only takes into account the average from 2015 to 2020.



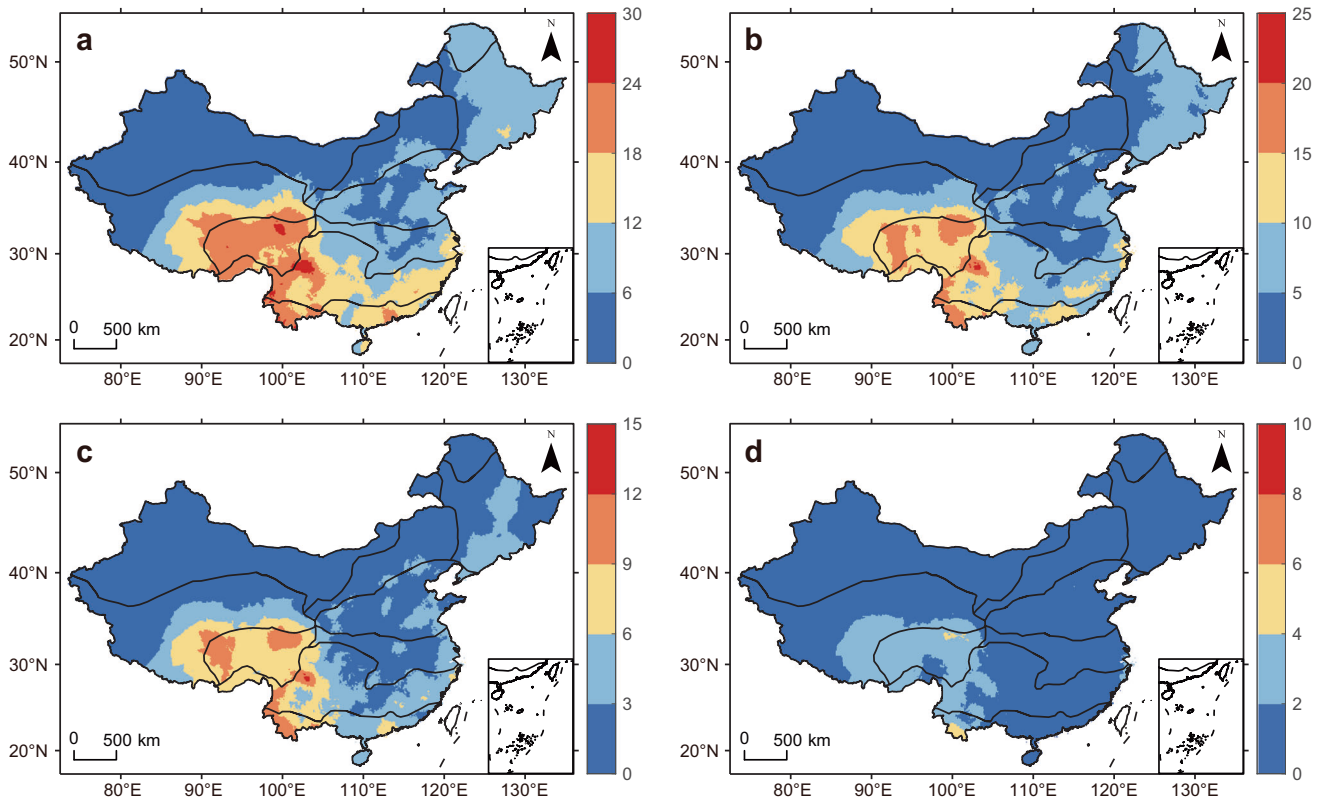


**Fig. 2 | Spatial patterns of SEPHCE (sequential extreme precipitation–heatwave compound events) frequency in China from 1975 to 2020. a** Spatial patterns of SEPHCE frequency at the 7-day interval; **b** spatial patterns of SEPHCE frequency at the 5-day interval; **c** spatial patterns of SEPHCE frequency at the 3-day interval; **d** spatial patterns of SEPHCE frequency at the 1-day interval.

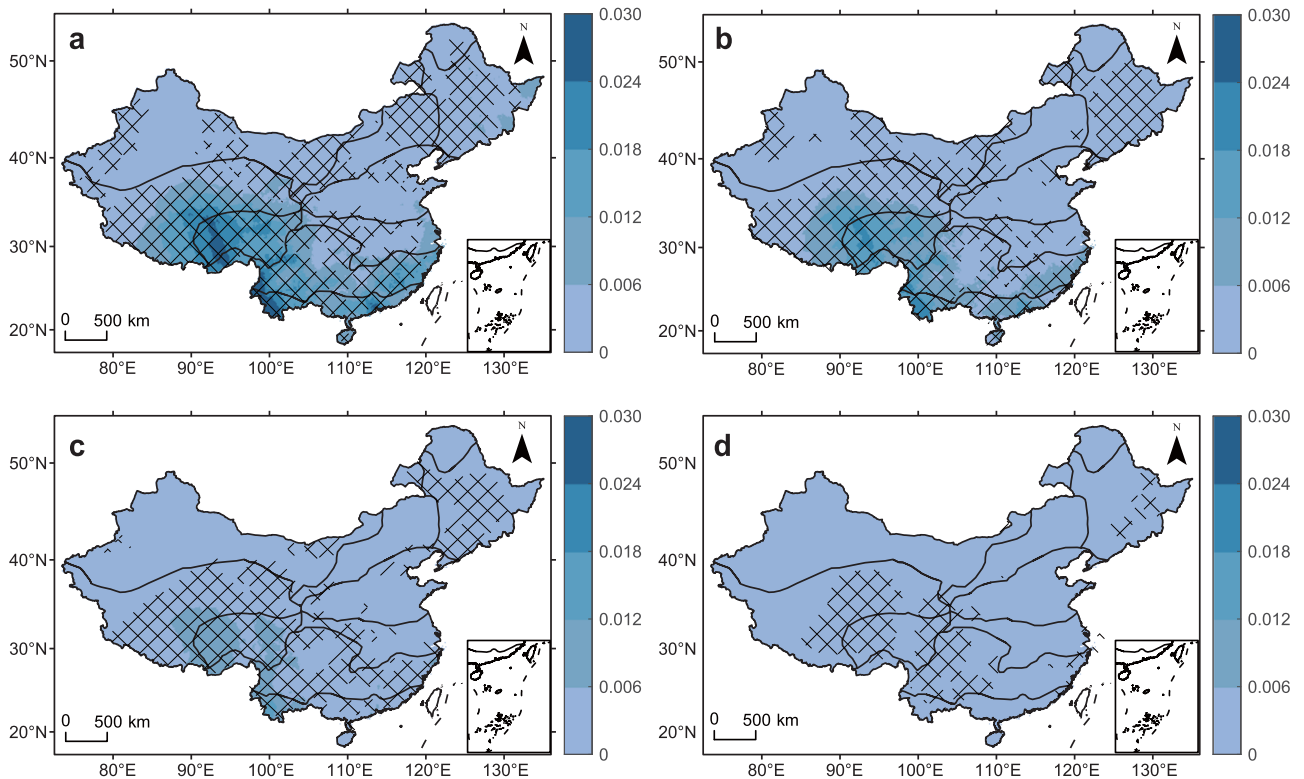


**Fig. 3 | Spatial trends of SEPHCE (sequential extreme precipitation–heatwave compound events) frequency in China from 1975 to 2020. a** Spatial trends of SEPHCE frequency at the 7-day interval; **b** spatial trends of SEPHCE frequency at the 5-day interval; **c** spatial trends of SEPHCE frequency at the 3-day interval; **d** spatial trends of SEPHCE frequency at the 1-day interval. The black squares show the variation trend was statistically significant at the 1% significance level.

**Fig. 4 | Annual variations of SEPHCE (sequential extreme precipitation–heatwave compound events) duration in China from 1975 to 2020.** **a** The annual SEPHCE duration; **b** the ratios of the mean SEPHCE duration in the latter 10 years to the former 10 years. Due to data limitations, the last mean ratio only takes into account the average from 2015 to 2020.

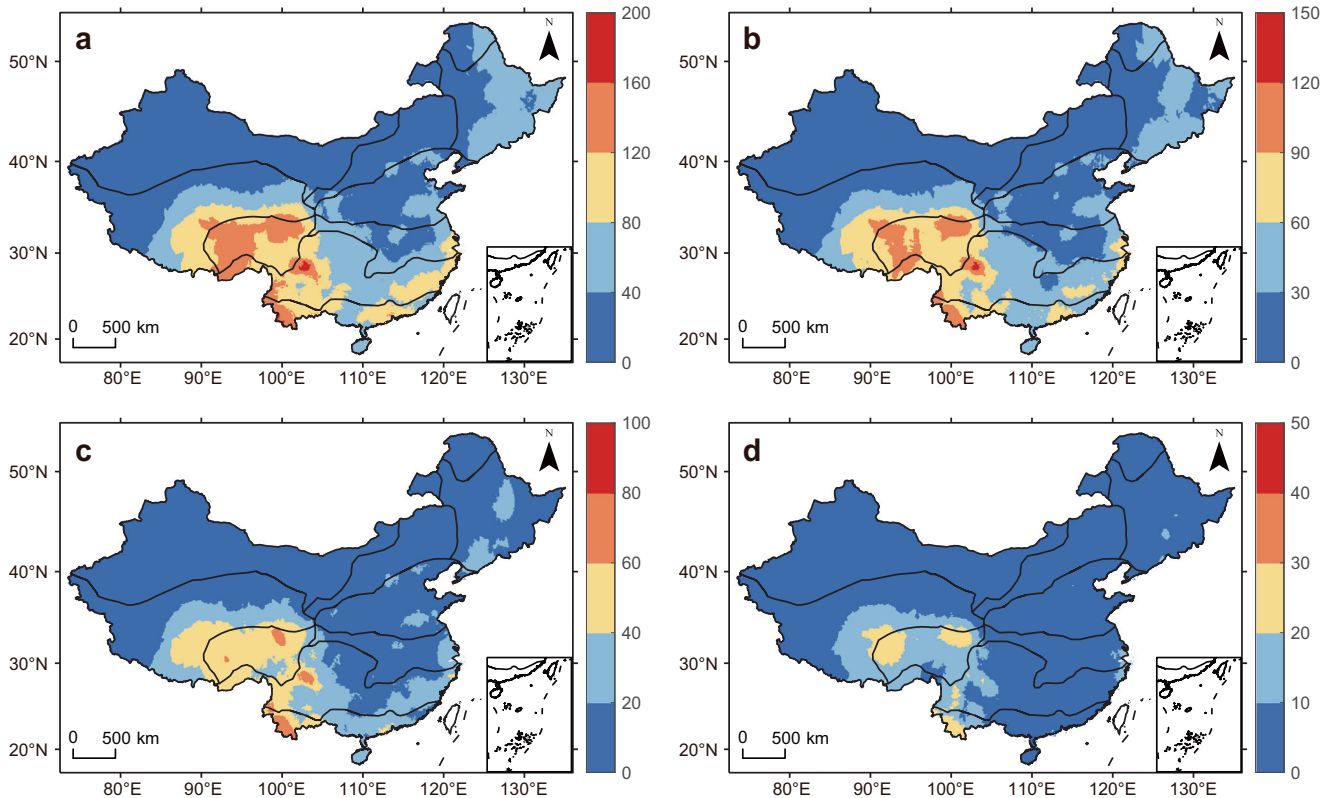
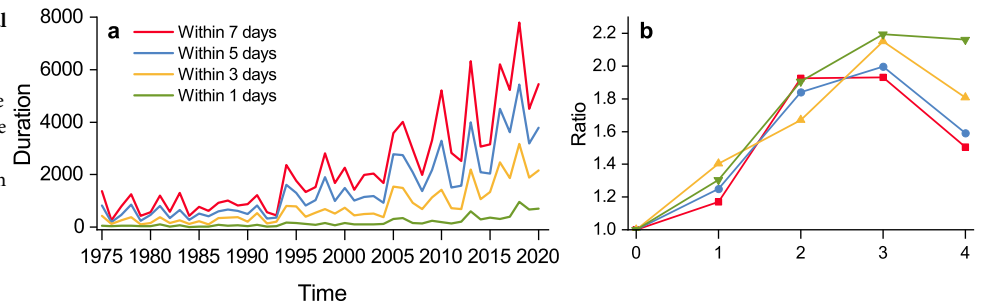


**Fig. 5 | Spatial patterns of SEPHCE (sequential extreme precipitation–heatwave compound events) duration in China from 1975 to 2020.** **a** Spatial patterns of SEPHCE duration at the 7-day interval; **b** spatial patterns of SEPHCE duration at the

5-day interval; **c** spatial patterns of SEPHCE duration at the 3-day interval; **d** spatial patterns of SEPHCE duration at the 1-day interval.

increase in SEPHCE duration occurred at the 7-day interval, reaching a maximum of 7791 days across the entire region in 2018 (Fig. 4a). The ratio of mean SEPHCE durations during the most recent 10-year period, compared to the preceding 10 years, initially experiences a rapid increase before showing a subtle decline (Fig. 4b). The ratio for the first four decades (1975–2014) continued to increase, rising from 1.4 times to 2.0 times. In the last ratio (2015–2020), it still remained highest at the 1-day interval, reaching 2.3 times, despite a slight decrease in the ratio across all time intervals (Fig. 4b).

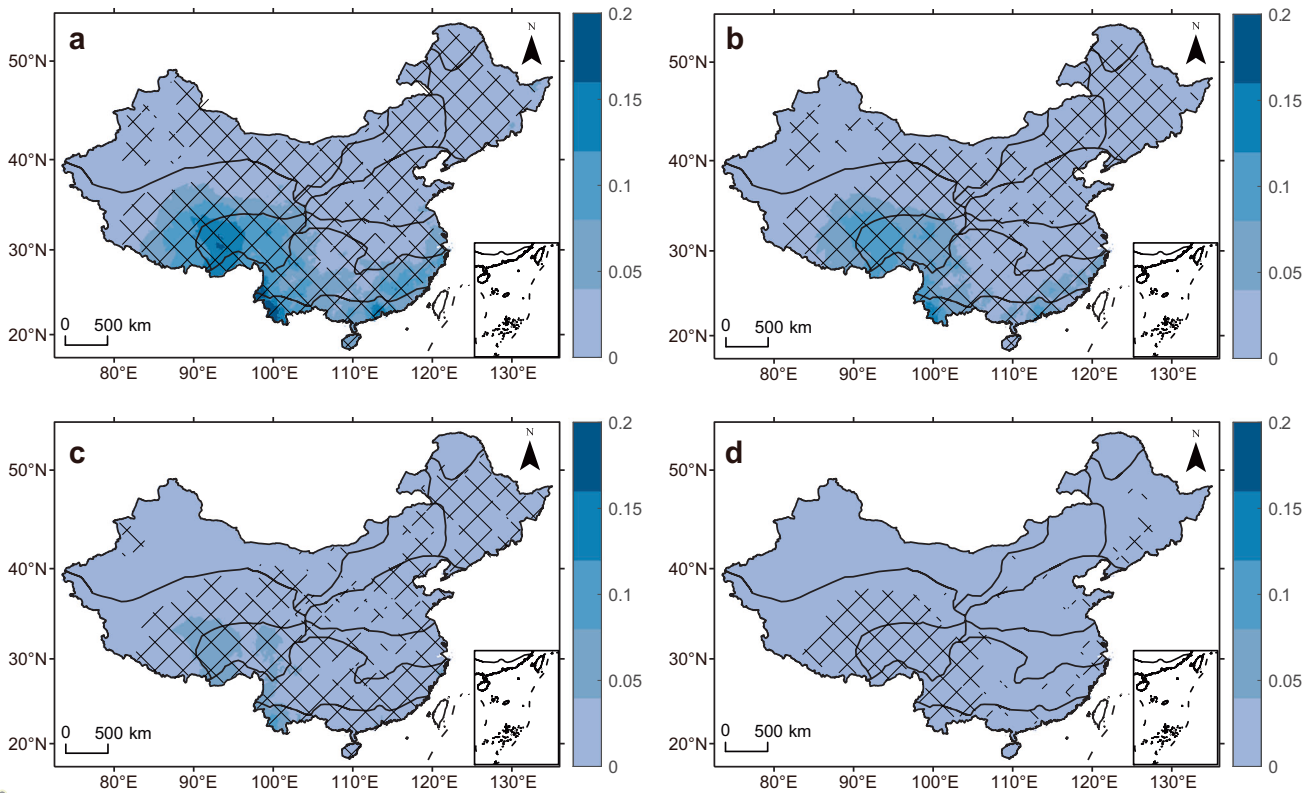
The SEPHCE duration in China from 1975 to 2020 exhibited distinct regional characteristics (Fig. 5). In general, SEPHCE duration was longer in the southwestern and southeastern coastal regions, while it was comparatively shorter in the northern areas (Fig. 5). With increasing time intervals, the duration extended, particularly in southwest China (Fig. 5). The spatial distribution of SEPHCE duration at the 5-day and 7-day intervals displayed similar patterns (Fig. 5a, b). In the south region, SEPHCE duration ranged from 80 to 160 days at the 7-day interval and from 60 to 120 days at the 5-day intervals (Fig. 5a, b). Conversely, SEPHCE duration was shorter in other regions, with a range of 6–80 days at the 7-day interval and 3–60 days at the

5-day interval (Fig. 5a, b). For the 3-day and 1-day intervals, longer SEPHCE durations were mainly concentrated in southwestern China, ranging from approximately 40 to 60 days at the 3-day interval and from 10 to 30 days at the 1-day interval (Fig. 5c, d).

From 1975 to 2020, it was observed that regions in southwestern and southern coastal China experienced a notably faster increase in SEPHCE duration, while other regions exhibited a relatively slower growth rate (Fig. 6). Specifically, the growth rate of SEPHCE durations at the 7-day interval was the most pronounced, with an increase ranging from 1 to 2 days per decade (Fig. 6a). In contrast, the durations of SEPHCE at the 5-day and 3-day intervals exhibited a relatively slower growth, ranging from 0.5 to 1.5 days per decade and from 0.5 to 1 day per decade (Fig. 6b, c). However, the trends of SEPHCE duration at the 1-day interval were not significant, remaining below 0.5 days per decade (Fig. 6d).

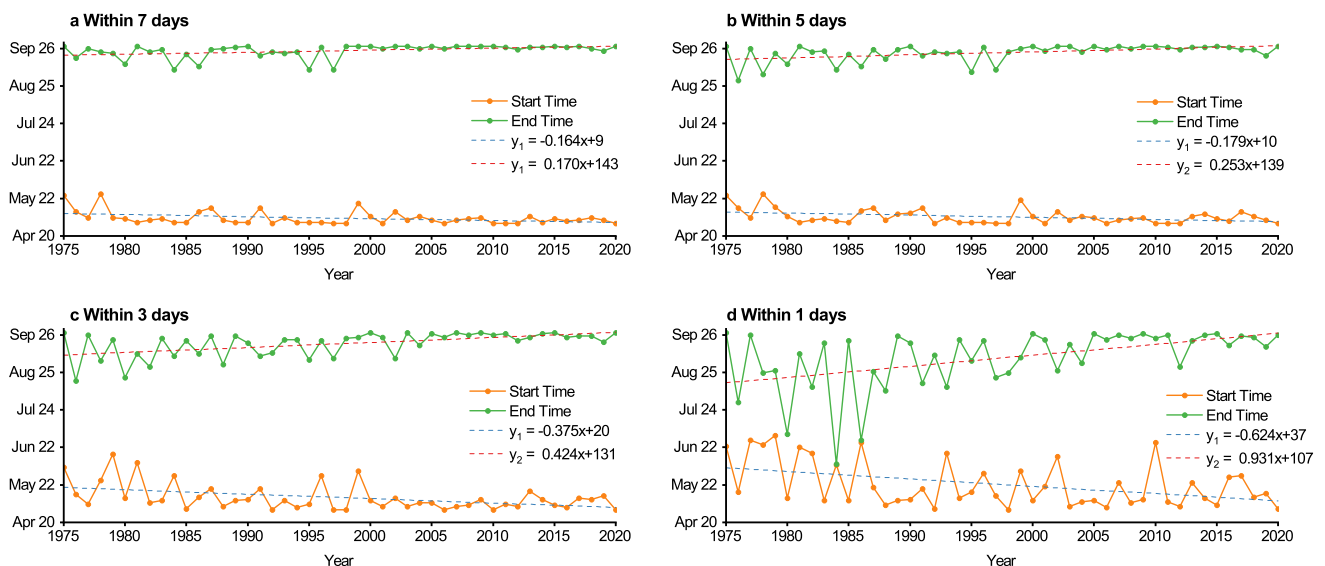
#### Annual variations in the starting and ending times of SEPHCE in China

Figure 7 illustrates the starting and ending times of SEPHCE fluctuations at various time intervals (1, 3, 5, and 7 days). Typically, SEPHCE began around



**Fig. 6 | Spatial trends of SEPHCE (sequential extreme precipitation–heatwave compound events) duration in China from 1975 to 2020. a** Spatial trends of SEPHCE duration at the 7-day interval; **b** spatial trends of SEPHCE duration at the

5-day interval; **c** spatial trends of SEPHCE duration at the 3-day interval; **d** spatial trends of SEPHCE duration at the 1-day interval. The black squares show the variation trend was statistically significant at the 1% significance level.



**Fig. 7 | Annual variations in the starting and ending times of SEPHCE (sequential extreme precipitation–heatwave compound events) in China from 1975 to 2020. a** Annual variations of the starting and ending times of SEPHCE at the 7-day interval; **b** annual variations of the starting and ending times of SEPHCE at the 5-day interval; **c** annual variations of the starting and ending times of SEPHCE at the 3-day

interval; **d** annual variations of the starting and ending times of SEPHCE at the 1-day interval. The orange line represents the starting time of SEPHCE for each year, while the green line represents the ending time of SEPHCE for each year, and the thin lines were their respective fitted curves.

the 3rd of May and concluded around 25th September (Fig. 7). Notably, there was a clear trend of advancing starting times and delaying ending times (Fig. 7a–d). The rate of advancement in the starting times significantly exceeded the rate of delay in the ending times (Fig. 7a–d). From 1975 to 2020, the advancement rate for the starting times was approximately

4.4 days per decade, while the delaying rate was approximately 3.3 days per decade (Fig. 7a–d). As the time interval decreases, this changing trend in the starting and ending times becomes more noticeable (Fig. 7a–d). Specifically, at the intervals of 1, 3, 5 and 7 days, the advancement rates for the SEPHCE starting times were approximately 9.3, 4.2, 2.5, and 1.7 days per decade,

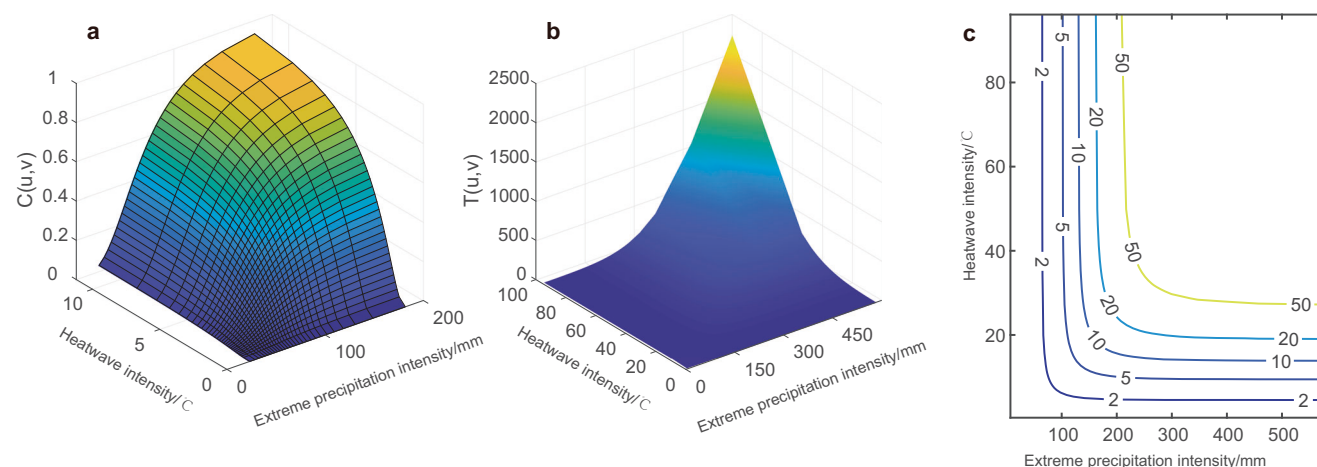


**Fig. 8 | The joint distribution and return periods of extreme precipitation intensity and heatwave intensity.** **a** The three-dimensional plots depict the joint probability distribution of extreme precipitation intensity and heatwave intensity

from 1975–2020; **b** the three-dimensional plot representing the joint return period distribution of extreme precipitation intensity and heatwave intensity, and **c** the contour plot of return periods for different years in China (2, 5, 10, 20, and 50 years).

respectively (Fig. 7a–d). The delay rates for ending times under these intervals were approximately 6.2, 3.7, 1.8, and 1.6 days per decade, respectively (Fig. 7a–d). These findings highlight the changes in the timing of SEPHCE over the years, with start times advancing and end times delaying, and this effect becomes more pronounced as the time intervals decrease.

#### Joint return period of extreme precipitation intensity and heatwave intensity in China

As both extreme precipitation intensity and heatwave intensity increase, the corresponding joint distribution probability also increases (Fig. 8a). However, unraveling the intricate linear relationship between the two proves to be complex. Here, the estimated value of the correlation parameter obtained by fitting the Gaussian Copula model ( $\rho_{\text{ohat}}$ ) is  $-0.049$ , indicating a weak negative correlation (Supplementary Fig. 3).

In Fig. 8b, as both extreme precipitation intensity and heatwave intensity increase, the joint return period of disasters also rises. On this 3D surface, the  $x$ -axis represents extreme precipitation intensity, the  $y$ -axis represents heatwave intensity, and the  $z$ -axis represents the return period of events where extreme precipitation intensity, heatwave intensity, or both exceed or are equal to a specified intensity (Fig. 8b). Figure 8c illustrates that as extreme precipitation intensity and heatwave intensity increase, joint return periods also increase. Simultaneously, the isopleths gradually become less dense, indicating a gradual rise in extreme precipitation and heatwave intensity (Fig. 8c).

#### Discussion

Previous studies have often examined extreme precipitation and heatwaves in isolation, neglecting a comprehensive investigation into their compound characteristics. This study provides evidence for compound events, specifically SEPHCE in China. A distinctive trend emerges, revealing an earlier onset and delayed cessation of SEPHCE, with the earlier onset trend surpassing that of delayed cessation. Particularly noteworthy is the pronounced trend in the worst-case scenario of SEPHCE (within 1 day), where both earlier onset and delayed cessation are most evident. This suggests an increased likelihood of this once rare compound event due to global warming, imposing heightened pressure from SEPHCE. Urgent attention is required to address the potential disastrous impacts on ecosystems and societal breakdowns arising from the current climate change emergency<sup>30,38</sup>.

While our study focuses on mainland China, the framework proposed can be applied globally to examine SEPHCE occurrences, provided there are reliable long-term temperature and precipitation datasets. Our research findings unequivocally indicate a consistent upward trend in the frequency and duration of SEPHCE in China from 1975 to 2020, with a notable

acceleration post-1993. This trend exhibits significant regional disparities, primarily concentrated in the southern China. These findings align with the observations of researchers such as Chen et al., who noted a 5–9 times increase in sequential flood–heatwave events in the past two decades, predominantly in the southeast and western China<sup>39</sup>. Notably, SEPHCE within shorter time intervals is relatively rare, with a smaller hotspot area. However, over the past decades, the frequency and duration of these short-interval SEPHCE have doubled every ten years, indicating a concerning and evolving trend that demands careful attention and further investigation.

Urban floods linked to extreme precipitation, flash floods in mountainous areas, and subsequent heatwaves pose serious threats to agriculture and human life<sup>21,40</sup>. Excessive precipitation may lead to disasters such as floods and landslides, causing infrastructure damage. When followed by a heatwave, crops may be affected, leading to reduced yields, and people may be at risk of heatstroke<sup>41</sup>. Especially in the southwestern region of China, with its complex terrain, relatively fragile ecosystems, and comparatively underdeveloped economy, it is more susceptible to the impact of SEPHCE, resulting in significant losses<sup>42</sup>. Therefore, it is essential for government to prioritize this issue and implement more urgent and effective measures to mitigate the unequal impacts of climate change on different regions while promoting sustainable development<sup>43</sup>.

The noticeable increase in SEPHCE is closely related to simultaneous rises in extreme precipitation and heatwaves<sup>44</sup>. They delve into the relative contributions of extreme precipitation and heatwaves to the increased occurrence of SEPHCE, finding that the increase in heatwaves leads to a more frequent simultaneous occurrence of these two independent extreme events<sup>44</sup>. The rise in heatwaves is mainly attributed to global warming, with IPCC AR6 noting an increasing attribution of global warming to external forcings from human activities<sup>4</sup>. Regarding regional variations, a detailed analysis of physical mechanisms suggests that tropical intraseasonal oscillations and meandering of subtropical may dynamically facilitate the consecutive occurrence of floods and heatwaves in southern China<sup>45,46</sup>. In the southeast coastal regions of China, strong summer typhoons provide another pathway for heatwaves following extreme precipitation, enhancing upper-level anticyclones and stabilizing the atmosphere through the delayed effect of non-adiabatic heating released by typhoons<sup>47–50</sup>. However, the seasonal distribution of precipitation is becoming increasingly uneven, potentially triggering a series of processes leading to the aggregation of extreme precipitation and heatwaves, transitioning rapidly from flash floods to drought, followed by drought-induced heatwaves<sup>51–53</sup>. While these potential physical connections are not currently robust and stable, further research is needed to gain a deeper understanding of these complex meteorological and climatic mechanisms.

Our research findings as both extreme precipitation intensity and heatwave intensity increase, the corresponding joint distribution probability also increases. However, unraveling the intricate linear relationship between the two proves to be complex<sup>21</sup>. The rise in temperature results in increased evaporation, causing a reduction in moisture and contributing to a rise in drought events<sup>40</sup>. Moreover, the enhanced atmospheric water-holding capacity, requiring more water vapor to saturate the air, leads to an increase in the frequency of extreme precipitation and the occurrence of extreme precipitation events<sup>21,54</sup>. Here, the estimated value of the correlation parameter obtained by fitting the Gaussian Copula model ( $\rho_{\text{ohat}}$ ) is  $-0.049$ , indicating a weak negative correlation, while there is also a possibility of a positive correlation. This explanation emphasizes the interaction between heatwaves and extreme precipitation, elucidating their relationship in terms of probability distribution.

## Methods

### Data

The observational datasets of daily maximum temperature, minimum temperature and precipitation data for 1975–2020 were sourced from the National Meteorological Information Center (NMIC), created by China Meteorological Administration (<http://data.cma.cn/>). This invaluable resource incorporates data information from a network of 2479 meteorological stations across mainland China. To detect SEPHCE, the primary study period was the extended summer months from May to September<sup>55</sup>. And we further enhanced data reliability through NMIC's data quality control measures, including checks for climate extremes, internal consistency, temporal consistency, and spatial consistency. We interpolated the missing values, and the number of missing values was controlled to be below 5% during the study period, that is, there were fewer than 7 missing values during the study period every year<sup>44</sup>. Finally, there were still 1929 useful stations for this study.

### The definition and of SEPHCE

The World Meteorological Organization notes that there was no universally accepted definition of heatwaves<sup>18</sup>. Various definitions, metrics, and indices have been proposed in the scientific literature and are adopted by meteorological departments and authoritative institutions. Some definitions are based on local criteria and absolute temperature thresholds, while others are calculated based on percentage standards relative to temperature<sup>44</sup>. However, variations in climatic characteristics across diverse regions and seasons can result in the definition based on absolute thresholds being deemed either “too high” or “too low”<sup>56</sup>. In contrast, the relative threshold is usually associated with the climatic conditions of specific regions and time frames<sup>57,58</sup>. Heatwaves identified using relative thresholds for high temperatures can capture unusually elevated temperatures in various seasons, offering a more precise characterization of local abnormal conditions<sup>49</sup>. Furthermore, some studies only consider daytime high temperatures to define heatwaves, it is vital to acknowledge that nighttime high temperatures also significantly impact human well-being<sup>21,59</sup>. The severest heatwaves occur when both daytime and nighttime temperatures are abnormally elevated<sup>60</sup>. Therefore, following the approach of Chen et al., we refined our definition of a heatwave event as a period lasting at least three consecutive days where the daily maximum and/or minimum temperature surpass the 90% percentile of the daily change threshold calculated within 15-day moving window (7 days before and after a specific day). This reference threshold is derived from a 30-year reference period (1975–2004), resulting in a dataset of 450 days with a 90th percentile, following the method of Della-Marta et al.<sup>61</sup>. Throughout our investigation, the mean threshold values for maximum and minimum temperature were 34.3 and 23.5 °C, respectively. Percentile-based thresholds, known for their reliability and widely applicability, have been extensively used in prior studies and can be applied universally on a global scale or to extended region such as the one under investigation<sup>24,44,56,62–65</sup>.

The Expert Team on Climate Change Detection and Indices employs various methods to define extreme precipitation<sup>66–70</sup>. The advantages lie in

standardization, robustness, and a comparatively high signal-to-noise ratio, facilitating cross-mode and cross-regional comparisons<sup>71</sup>. Given China's extensive geographical diversity across multiple climate zones, a relative threshold approach is applied to define extreme precipitation events<sup>72</sup>. To comprehensively capture precipitation extremes, we use a 95% threshold and daily precipitation as the criteria for extreme events<sup>73</sup>. Consequently, we refined an extreme precipitation event as a daily precipitation exceeding that of 95% of all rain days during a reference period<sup>74</sup>. The reference period for extreme precipitation coincides with that of heatwave, covering the summer period (May–September) from 1975 to 2004. Throughout the study period, the average rainfall threshold across all regions was 44.5 mm day<sup>-1</sup>, classifying it as heavy rain according to the precipitation categorization established by the China Meteorological Administration. This definition method was also widely adopted by numerous scholars<sup>21,75–77</sup>.

A SEPHCE is defined as the occurrence of extreme precipitation followed by a heatwave event within a specific time interval<sup>78</sup>. For our analysis, we examined various time intervals, including 7-day, 5-day, 3-day, and 1-day intervals<sup>21,44</sup>. Specifically, a SEPHCE at the 7-day interval indicates that a heatwave occurs seven days after the conclusion of extreme precipitation. In our analysis, we implemented a rule to address scenarios where a single extreme precipitation event is followed by multiple heatwave events or where multiple extreme precipitation events are followed by heatwaves. In such cases, we only consider the first extreme precipitation event and the first heatwave event<sup>21</sup>, simplifying the analysis and preventing redundancy or data overlap.

SEPHCE frequency denotes the total occurrences of SEPHCE nationwide from 1975 to 2020. Temporal trends in SEPHCE frequency are measured by counting the annual occurrences at 1929 stations. Additionally, we calculate the ratio of 10-year averages. The first ratio involves finding the mean SEPHCE frequency from 1985 to 1994, and then calculating the mean frequency from 1975 to 1984. This ratio between these two means represents the ratio of the latter 10 years to the former 10 years. This process is repeated, resulting in a total of 4 ratios. The last ratio accounts for the 6-year SEPHCE frequency mean from 2015 to 2020 due to the limited time period. The spatial distribution of SEPHCE frequency involves interpolating the annual SEPHCE frequency for each station into a grid of 0.1° longitude × 0.1° latitude covering mainland China. We aggregated the SEPHCE frequency data for 46 years to calculate the total counts for each grid. The spatial variation trend of SEPHCE frequency is also interpolated into a grid of 0.1° longitude × 0.1° latitude for mainland China. We used the Sen Median method to calculate the variation trend of SEPHCE frequency over 46 years for each grid and the Mann–Kendall (MK) test. SEPHCE duration refers to the cumulative duration of SEPHCE nationwide from 1975 to 2020. The duration includes the sum of the duration of extreme precipitation events and heatwave events within each SEPHCE. Temporal trends in SEPHCE duration involves calculating the yearly duration at 1929 stations. Similar to SEPHCE frequency, we also calculate the mean for each 10-year period and the ratio of the mean for the latter 10 years to the mean for the former 10 years. Additionally, we study the spatial distribution and variation trend of SEPHCE duration. The start and end times of SEPHCE are defined as the earliest start time among SEPHCE and the latest end time of SEPHCE at each station annually<sup>79</sup>. The intensity of heatwaves is determined as the difference between the annual maximum and minimum temperatures and their respective thresholds<sup>21</sup>. The intensity of extreme precipitation is defined as the cumulative precipitation during extreme precipitation events within each compound event.

### Trend analysis and significance testing

We employed the robust non-parametric statistical method known as Theil–Sen Median trend analysis, along with the MK test, to calculate the changing trends in the frequency and duration of SEPHCE<sup>80</sup>. This method has been widely used to calculate changing trends in extreme weather. The Theil–Sen Median method, also known as Sen slope estimation, boasts high computational efficiency<sup>81</sup>. It is insensitive to measurement errors and outlier data, which makes it suitable for trend analysis of long time series

data. The formula for the Sen slope was as follows:

$$\beta = \text{Median} \left( \frac{x_j - x_i}{j - i} \right), \forall j > i \quad (1)$$

In the formula, if  $\beta$  is greater than zero, it indicates an increase in the frequency or duration of SEPHCE, and conversely when  $\beta$  is less than zero.

The MK test is a non-parametric method for assessing time series trends. It does not rely on the assumption that the measured values follow a normal distribution, and it is robust against missing values or outliers. This makes it suitable for testing the significance of trends in long time series data. The index data is considered in sequence by time  $X = \{x_1, x_2, \dots, x_n\}$  ( $n \geq i > j \geq 1$ ), and the MK test was calculated as follows:

$$\text{MK} = \sum_{i=1}^{n-1} \sum_{j=i+1}^n f(x_j - x_i) \quad (2)$$

where  $f(x_i - x_j) = 1$ , when  $(x_i - x_j) > 0$ ;  $f(x_i - x_j) = 0$ , when  $(x_i - x_j) = 0$ ; and  $f(x_i - x_j) = -1$ , when  $(x_i - x_j) < 0$ . The indicator follows an upward trend when  $\text{MK} > 0$ , a downward trend when  $\text{MK} < 0$ , and no change in trend when  $\text{MK} = 0$ ; the larger the absolute value of MK, the more severe the trend.

### Copula function for capturing the joint probability distribution of SEPHCE

Quantifying the intensity of compound events that involve concurrent extreme precipitation and heatwaves is challenging. However, it is possible to quantify the intensities of extreme precipitation and heatwaves individually. In this study, Copula functions are employed to quantify the probability of joint distribution of extreme precipitation and heatwave intensities within compound events<sup>82</sup>. It also aims to determine their return periods. Copula analysis is a widely used technique in geoscience research, including hydrological frequency analysis<sup>83,84</sup> and regional drought analysis<sup>85</sup>.

The present study used copula functions to create an extreme precipitation intensities - heatwaves intensities bivariate distribution. So, technically, the copula approach divides the problem into two mutually independent steps concerning fitting the marginal distributions and finding the dependence structure among the margins. First, we used five univariate distribution functions were fitted to the extreme precipitation and heatwaves intensities data. Subsequently, we estimated the parameters of these distribution models using the maximum likelihood method. Ultimately, we found that the optimal distribution model for extreme precipitation intensity is the generalized extreme value distribution, while the optimal model for heatwave intensity is the logarithmic distribution. The distribution functions adopted in this research are listed in Supplementary Table 1.

We further utilized four bivariate copula functions, including Gaussian, Gumbel, Clayton, and Frank to fit the marginal distributions and create the joint probability of extreme precipitation intensity and heatwave intensity. Based on the results of the OLS test, we selected the optimal joint distribution model, which is the Gaussian function distribution. Copula families adopted in this research are listed in Supplementary Table 2.

Planning and management of SEPHCE under climate change requires estimates based on the return period of SEPHCE. According to the joint probability distribution of SEPHCE, return periods for  $P \geq p$  and  $H \geq h$  as  $T_{PH}$  is defined for base and future periods where  $F_P(p)$  and  $F_H(h)$  are the cumulative distribution functions of extreme precipitation intensity and heatwave intensity,  $C$  is the copula function, and  $E(L)$  is the average inter-arrival time, which can be estimated from the observed SEPHCE<sup>86</sup>.

$$T_{PH} = \frac{E(L)}{P(P \geq p, H \geq h)} = \frac{E(L)}{1 - F_P(p) - F_H(h) + C(F_P(p), F_H(h))} \quad (3)$$

### Data availability

The meteorological data are retrieved from the National Meteorological Information Center (NMIC), at <http://data.cma.cn/>.

### Code availability

The source codes for the analysis of this study are available from the corresponding author upon reasonable request.

Received: 8 November 2023; Accepted: 28 February 2024;

Published online: 11 March 2024

### References

- Wang, Q. et al. Freeze-thaw cycle representation alters response of watershed hydrology to future climate change. *CATENA* **195**, 104767 (2020).
- Xu, F. et al. Understanding climate change impacts on drought in China over the 21st century: a multi-model assessment from CMIP6. *npj Clim. Atmos. Sci.* **7**, 32 (2024).
- Wan, L. et al. Drought characteristics and dominant factors across China: insights from high-resolution daily SPEI dataset between 1979 and 2018. *Sci. Total Environ.* **901**, 166362 (2023).
- IPCC. *Climate Change 2021: The Physical Science Basis* (Cambridge University Press, 2021).
- Wu, X. et al. The effect of drought on vegetation gross primary productivity under different vegetation types across China from 2001 to 2020. *Remote Sens.* **14**, 4658 (2022).
- WEF. *The Global Risks Report 2020* (WEF, 2020).
- UNDRR. *The Human Cost of Disasters: An Overview of the Last 20 Years (2000-2019)* (United Nations Office for Disaster Risk Reduction, Centre for Research on the Epidemiology of Disasters, 2020).
- Department, D. R. a. M. S. *The Ministry of Emergency Management has released the nationwide natural disaster situation report for November 2023*. Available at: <https://www.mem.gov.cn/xw/yjglbgzdt> (Ministry of Emergency Management of the People's Republic of China, Beijing, 2023).
- Li, W. et al. Anthropogenic impact on the severity of compound extreme high temperature and drought/rain events in China. *npj Clim. Atmos. Sci.* **6**, 79 (2023).
- IPCC. *Climate Change 2013: The Physical Science Basis* (Cambridge University Press, 2013).
- Zscheischler, J. et al. Impact of large-scale climate extremes on biospheric carbon fluxes: an intercomparison based on MsTMIP data. *Glob. Biogeochem. Cycles* **28**, 585–600 (2014).
- Zscheischler, J. et al. Future climate risk from compound events. *Nat. Clim. Change* **8**, 469–477 (2018).
- Cowan, T. et al. Forecasting the extreme rainfall, low temperatures, and strong winds associated with the northern Queensland floods of February 2019. *Weather Clim. Extremes* **26**, 100232 (2019).
- Zhang, W. & Villarini, G. Deadly compound heat stress-flooding hazard across the central United States. *Geophys. Res. Lett.* **47**, e2020GL089185 (2020).
- Fu, J. et al. Extreme rainfall reduces one-twelfth of China's rice yield over the last two decades. *Nat. Food* **4**, 416–426 (2023).
- Lüthi, S. et al. Rapid increase in the risk of heat-related mortality. *Nat. Commun.* **14**, 4894 (2023).
- Newman, R. & Noy, I. The global costs of extreme weather that are attributable to climate change. *Nat. Commun.* **14**, 6103 (2023).
- WMO. *WMO Atlas of Mortality and Economic Losses from Weather, Climate and Water Extremes (1970–2019)* (WMO, 2021).
- Wang, S. S. et al. Consecutive extreme flooding and heat wave in Japan: are they becoming a norm? *Atmos. Sci. Lett.* **20**, e933 (2019).
- Imada, Y., Watanabe, M., Kawase, H., Shiogama, H. & Arai, M. The July 2018 high temperature event in Japan could not have happened



- without human-induced global warming. *Sci. Online Lett. Atmos.* **15A**, 8–12 (2019).
21. You, J. & Wang, S. Higher probability of occurrence of hotter and shorter heat waves followed by heavy rainfall. *Geophys. Res. Lett.* **48**, e2021GL094831 (2021).
  22. Ridder, N. N. et al. Global hotspots for the occurrence of compound events. *Nat. Commun.* **11**, 5956 (2020).
  23. Gu, L. et al. Global increases in compound flood-hot extreme hazards under climate warming. *Geophys. Res. Lett.* **49**, e2022GL097726 (2022).
  24. Liao, Z., Chen, Y., Li, W. & Zhai, P. Growing threats from unprecedented sequential flood-hot extremes across China. *Geophys. Res. Lett.* **48**, e2021GL094505 (2021).
  25. Leng, G., Tang, Q., Huang, S. & Zhang, X. Extreme hot summers in China in the CMIP5 climate models. *Clim. Change* **135**, 669–681 (2016).
  26. Zhou, P. & Liu, Z. Likelihood of concurrent climate extremes and variations over China. *Environ. Res. Lett.* **13**, 094023 (2018).
  27. Ren, G. & Zhou, Y. Urbanization effect on trends of extreme temperature indices of national stations over Mainland China, 1961–2008. *J. Clim.* **27**, 2340–2360 (2014).
  28. Sun, Y. et al. Contribution of global warming and urbanization to changes in temperature extremes in Eastern China. *Geophys. Res. Lett.* **46**, 11426–11434 (2019).
  29. Matthews, T., Wilby, R. L. & Murphy, C. An emerging tropical cyclone–deadly heat compound hazard. *Nat. Clim. Change* **9**, 602–606 (2019).
  30. Wasko, C. Review: Can temperature be used to inform changes to flood extremes with global warming? *Philos. Trans. Ser. A Math. Phys. Eng. Sci.* **379**, 20190551 (2021).
  31. Wang, Q. et al. A multi-scale daily SPEI dataset for drought characterization at observation stations over mainland China from 1961 to 2018. *Earth Syst. Sci. Data* **13**, 331–341 (2021).
  32. Zeng, J. et al. Improving the drought monitoring capability of VHI at the global scale via ensemble indices for various vegetation types from 2001 to 2018. *Weather Clim. Extremes* **35**, 100412 (2022).
  33. Zhang, R. et al. The first high spatial resolution multi-scale daily SPI and SPEI raster dataset for drought monitoring and evaluating over China from 1979 to 2018. *Big Earth Data* **7**, 1–26 (2023).
  34. Marshall, A. G. et al. Intra-seasonal drivers of extreme heat over Australia in observations and POAMA-2. *Clim. Dyn.* **43**, 1915–1937 (2014).
  35. Feudale, L. & Shukla, J. Influence of sea surface temperature on the European heat wave of 2003 summer. Part I: an observational study. *Clim. Dyn.* **36**, 1691–1703 (2011).
  36. Perkins, S. E. A review on the scientific understanding of heatwaves—their measurement, driving mechanisms, and changes at the global scale. *Atmos. Res.* **164–165**, 242–267 (2015).
  37. UN. *Surprise Early Heatwave in Europe, Harbinger of Things to Come* (United Nations, 2022).
  38. de Ruiter, M. C. et al. Why we can no longer ignore consecutive disasters. *Earth's Future* **8**, e2019EF001425 (2020).
  39. Chen, Y., Zhou, B., Zhai, P. & Moufouma-Okia, W. Half-a-degree matters for reducing and delaying global land exposure to combined daytime-nighttime hot extremes. *Earth's Future* **7**, 953–966 (2019).
  40. Zeng, Z. et al. Increased risk of flash droughts with raised concurrent hot and dry extremes under global warming. *npj Clim. Atmos. Sci.* **6**, 134 (2023).
  41. Kim, H. et al. *Flood and Heatwave in Japan 2018 and Future Increase of Consecutive Compound Risk in a Warmer World* (American Geophysical Union, 2019).
  42. Bing, G., Lin, J., Wei, L., Guang, Y. & Dazhuan, G. Study of an evaluation method of ecosystem vulnerability based on remote sensing in a southwestern karst mountain area under extreme climatic conditions. *Acta Ecol. Sin.* **37**, 7219–7231 (2017).
  43. AghaKouchak, Amir et al. How do natural hazards cascade to cause disasters? *Nature* **7724**, 458–460 (2018).
  44. Chen, Y., Liao, Z., Shi, Y., Tian, Y. & Zhai, P. Detectable increases in sequential flood-heatwave events across China during 1961–2018. *Geophys. Res. Lett.* **48**, e2021GL092549 (2021).
  45. Chen, Y. & Zhai, P. Simultaneous modulations of precipitation and temperature extremes in Southern parts of China by the boreal summer intraseasonal oscillation. *Clim. Dyn.* **49**, 3363–3381 (2017).
  46. Li, R. C. Y. & Zhou, W. Modulation of western north pacific tropical cyclone activity by the ISO. Part I: genesis and intensity. *J. Clim.* **26**, 2904–2918 (2013).
  47. Hart, R. E., Maue, R. N. & Watson, M. C. Estimating local memory of tropical cyclones through MPI anomaly evolution. *Mon. Weather Rev.* **135**, 3990–4005 (2007).
  48. McTaggart-Cowan, R., Bosart, L. F., Gyakum, J. R. & Atallah, E. H. Hurricane Katrina (2005). Part II: evolution and hemispheric impacts of a diabatically generated warm pool. *Mon. Weather Rev.* **135**, 3927–3949 (2007).
  49. Parker, T. J., Berry, G. J. & Reeder, M. J. The influence of tropical cyclones on heat waves in Southeastern Australia. *Geophys. Res. Lett.* **40**, 6264–6270 (2013).
  50. Pun, I. F., Hsu, H. H., Moon, I. J., Lin, I. I. & Jeong, J. Y. Marine heatwave as a supercharger for the strongest typhoon in the East China Sea. *npj Clim. Atmos. Sci.* **6**, 128 (2023).
  51. Chen, Y. Increasingly uneven intra-seasonal distribution of daily and hourly precipitation over Eastern China. *Environ. Res. Lett.* **15**, 104068 (2020).
  52. Pendergrass, A. G. & Knutti, R. The uneven nature of daily precipitation and its change. *Geophys. Res. Lett.* **45**, 11,980–911,988 (2018).
  53. Miralles, D. G., Teuling, A. J., van Heerwaarden, C. C. & Vilà-Guerau de Arellano, J. Mega-heatwave temperatures due to combined soil desiccation and atmospheric heat accumulation. *Nat. Geosci.* **7**, 345–349 (2014).
  54. Wang, G. et al. The peak structure and future changes of the relationships between extreme precipitation and temperature. *Nat. Clim. Change* **7**, 268–274 (2017).
  55. Kalkstein, L. S. et al. Analog European heat waves for U.S. cities to analyze impacts on heat-related mortality. *Bull. Am. Meteorol. Soc.* **89**, 75–86 (2008).
  56. Perkins, S. E. & Alexander, L. V. On the measurement of heat waves. *J. Clim.* **26**, 4500–4517 (2013).
  57. Russo, S. et al. Magnitude of extreme heat waves in present climate and their projection in a warming world. *J. Geophys. Res. Atmos.* **119**, 12,500–512,512 (2014).
  58. Wang, P. et al. Heat waves in China: definitions, leading patterns, and connections to large-scale atmospheric circulation and SSTs. *J. Geophys. Res. Atmos.* **122**, 10,679–610,699 (2017).
  59. Li, Y., Ding, Y. & Liu, Y. Mechanisms for regional compound hot extremes in the mid-lower reaches of the Yangtze River. *Int. J. Climatol.* **41**, 1292–1304 (2021).
  60. Luo, M., Lau, N. C. & Liu, Z. Different mechanisms for daytime, nighttime, and compound heatwaves in southern China. *Weather Clim. Extremes* **36**, 100449 (2022).
  61. Della-Marta, P., Haylock, M., Luterbacher, J. & Wanner, H. Doubled length of western European summer heat waves since 1880. *J. Geophys. Res.* <https://doi.org/10.1029/2007JD008510> (2007).
  62. Ning, G. et al. Rising risks of compound extreme heat-precipitation events in China. *Int. J. Climatol.* **42**, 5785–5795 (2022).
  63. Casanueva, A. et al. Daily precipitation statistics in a EURO-CORDEX RCM ensemble: added value of raw and bias-corrected high-resolution simulations. *Clim. Dyn.* **47**, 719–737 (2016).
  64. Perkins-Kirkpatrick, S. E. & Lewis, S. C. Increasing trends in regional heatwaves. *Nat. Commun.* **11**, 3357 (2020).

65. Sun, Q., Miao, C., AghaKouchak, A. & Duan, Q. Unraveling anthropogenic influence on the changing risk of heat waves in China. *Geophys. Res. Lett.* **44**, 5078–5085 (2017).
66. Zhang, X. et al. Indices for monitoring changes in extremes based on daily temperature and precipitation data. *WIREs Clim. Change* **2**, 851–870 (2011).
67. Rojpratak, S. & Supharatid, S. Regional extreme precipitation index: evaluations and projections from the multi-model ensemble CMIP5 over Thailand. *Weather Clim. Extremes* **37**, 100475 (2022).
68. Sun, S. et al. Evolution of future precipitation extremes: viewpoint of climate change classification. *Int. J. Climatol.* **42**, 1220–1230 (2022).
69. Sillmann, J., Kharin, V. V., Zhang, X., Zwiers, F. W. & Bronaugh, D. Climate extremes indices in the CMIP5 multimodel ensemble: Part 1. Model evaluation in the present climate. *J. Geophys. Res. Atmos.* **118**, 1716–1733 (2013).
70. Yin, H. & Sun, Y. Characteristics of extreme temperature and precipitation in China in 2017 based on ETCCDI indices. *Adv. Clim. Change Res.* **9**, 218–226 (2018).
71. Alexander, L. V. et al. In *Managing the Risks of Extreme Events and Disasters to Advance Climate Change Adaptation: Special Report of the Intergovernmental Panel on Climate Change* (eds Barros, V., Qin, D., Christopher, B. F. & Stocker, T. F.) Ch. 3 (Cambridge University Press, 2012).
72. Sun, Q., Miao, C. & Duan, Q. Extreme climate events and agricultural climate indices in China: CMIP5 model evaluation and projections. *Int. J. Climatol.* **36**, 43–61 (2016).
73. Xiao, M., Zhang, Q. & Singh, V. P. Spatiotemporal variations of extreme precipitation regimes during 1961–2010 and possible teleconnections with climate indices across China. *Int. J. Climatol.* **37**, 468–479 (2017).
74. Zhai, P., Zhang, X., Wan, H. & Pan, X. Trends in total precipitation and frequency of daily precipitation extremes over China. *J. Clim.* **18**, 1096–1108 (2005).
75. Fang, H., Qiao, Y. & Jian, M. Dynamic and thermodynamic causes of summer extreme precipitation over South China. *Atmos. Res.* **293**, 106894 (2023).
76. Liu, Z., Gao, T., Zhang, W. & Luo, M. Implications of the Pacific meridional mode for summer precipitation extremes over China. *Weather Clim. Extremes* **33**, 100359 (2021).
77. Xia, J., Yang, X. Y., Liu, J., Wang, M. & Li, J. Dominant change pattern of extreme precipitation and its potential causes in Shandong Province, China. *Sci. Rep.* **12**, 858 (2022).
78. Leonard, M. et al. A compound event framework for understanding extreme impacts. *WIREs Clim. Change* **5**, 113–128 (2014).
79. Guo, X. et al. Variations in the start, end, and length of extreme precipitation period across China. *Int. J. Climatol.* **38**, 2423–2434 (2018).
80. Sen, P. K. Estimates of the regression coefficient based on Kendall's tau. *J. Am. Stat. Assoc.* **63**, 1379–1389 (1968).
81. Mann, H. B. Nonparametric tests against trend. *Econometrica* **13**, 245–259 (1945).
82. Durante, F. & Sempi, C. In *Copula Theory and Its Applications* (eds Jaworski, P., Durante, F., Härdle, W. K. & Rychlik, T.) 3–31 (Springer Berlin Heidelberg, 2010).
83. Liu, M., Yang, L., Smith, J. A. & Vecchi, G. A. Response of extreme rainfall for landfalling tropical cyclones undergoing extratropical transition to projected climate change: Hurricane Irene (2011). *Earth's Future* **8**, e2019EF001360 (2020).
84. Liu, Y. R., Li, Y. P., Ma, Y., Jia, Q. M. & Su, Y. Y. Development of a Bayesian-copula-based frequency analysis method for hydrological risk assessment – The Naryn River in Central Asia. *J. Hydrol.* **580**, 124349 (2020).
85. Ayantobo, O. O., Li, Y. & Song, S. Copula-based trivariate drought frequency analysis approach in seven climatic sub-regions of mainland China over 1961–2013. *Theor. Appl. Climatol.* **137**, 2217–2237 (2019).
86. Shiau, J. T. Fitting drought duration and severity with two-dimensional Copulas. *Water Resour. Manag.* **20**, 795–815 (2006).

## Acknowledgements

This research was kindly supported by the National Natural Science Foundation of China (U2342208, 42101295 and 41701103), the Natural Science Foundation of Jiangsu Province (BK20210657), the Startup Foundation for Introducing Talent of NUIST (2023r132), and the Postgraduate Research & Practice Innovation Program of Jiangsu Province (KYCX23\_1294). Q.L. expresses gratitude to the Jiangsu Province Distinguished Professor Program for its generous support.

## Author contributions

L.M. and L.J. designed the research; L.M., L.J., S.S., and Q.L. performed the research; E.A., R.L., and Y.Z. contributed new reagents/analytic tools; L.M. and L.J. analyzed data; L.M., L.J., S.S., E.A., Q.W., Z.Z., Y.L., and Q.L. wrote the paper.

## Competing interests

The authors declare no competing interests.

## Additional information

**Supplementary information** The online version contains supplementary material available at <https://doi.org/10.1038/s41612-024-00613-5>.

**Correspondence** and requests for materials should be addressed to Qiang Liu.

**Reprints and permissions information** is available at <http://www.nature.com/reprints>

**Publisher's note** Springer Nature remains neutral with regard to jurisdictional claims in published maps and institutional affiliations.

**Open Access** This article is licensed under a Creative Commons Attribution 4.0 International License, which permits use, sharing, adaptation, distribution and reproduction in any medium or format, as long as you give appropriate credit to the original author(s) and the source, provide a link to the Creative Commons licence, and indicate if changes were made. The images or other third party material in this article are included in the article's Creative Commons licence, unless indicated otherwise in a credit line to the material. If material is not included in the article's Creative Commons licence and your intended use is not permitted by statutory regulation or exceeds the permitted use, you will need to obtain permission directly from the copyright holder. To view a copy of this licence, visit <http://creativecommons.org/licenses/by/4.0/>.

© The Author(s) 2024